Nat Hazards (2011) 59:749–769
DOI 10.1007/s11069-011-9793-9

ORIGINAL PAPER

# Water storage loss in central and south Asia from GRACE satellite gravity: correlations with climate data

**Natthachet Tangdamrongsub · Cheinway Hwang · Yu-Chi Kao**

Received: 5 October 2010 / Accepted: 17 March 2011 / Published online: 30 March 2011


**Abstract** Recent decrease of water supply in central Asia and south Asia affects billions of people here. By filtering the errors at higher frequency components and correcting for the contaminated components, we enhance the monthly GRACE gravity fields to improve the determination of change in equivalent water height (EWH). The water storage changes from GRACE and the GLDAS hydrology model all show decreasing trends in this region. At the annual and inter-annual time scales, significant correlations between the variations in EWH and the variations in temperature, precipitation and snow equivalent height are found, especially at high altitude stations, suggesting that climate change is the driving factor for the water depletion in central Asia and south Asia.

**Keywords** Equivalent water height · Central Asia · South Asia · GRACE · Gravity · GLDAS

## 1 Introduction

The Asia continent contains several large water-supplying sources that feed more than 2 billion people here. Continual melting of the snow and ice over the mountain ranges in Asia may cause a severe shortage of water sooner than expected. With a climate change that could affect a population of 1,726,000,000 and 597,000,000 in central Asia and south Asia, respectively (based on 2009 world population data sheet), more promising climate data than what are available now in this region are needed to remove public concerns. For example, an official from the United Nation apologized for data errors in glacier retreats over the Himalayas on January 20, 2010. Glacier, ice and snow melting are main supplies of fresh water to the downstream areas of mountain ranges such as Tian Shan and the Himalayas. However, glaciers with area smaller than 0.5 $km^2$ in this region have lost their surface coverage larger than 4 times in the second half of 1963–2000

N. Tangdamrongsub · C. Hwang (✉) · Y.-C. Kao
Department of Civil Engineering, National Chiao Tung University,
1001 University Road, Hsinchu 300, Taiwan
e-mail: cheinway@mail.nctu.edu.tw; cheinway@gmail.com
URL: http://www.space.cv.nctu.edu.tw

(Niederer et al. 2008), inevitably affecting living activities of the people in this region (Kirby A., 'Kazakhstan's glaciers 'melting fast', BBC, 4 September 2003).

Tajikistan, one of the central Asia countries, does not only undergo with the economic problem but also suffers from a severe drought (Golovnina M., 'Tajikistan battles drought', The New York Times, 12 June 2008). Unfortunately, no local climatic data have been recorded in this area; only some existing scientific evidence provides us that the rise of temperature and melting of glaciers are responsible for the droughts over the region (Baker A., 'Climate change and water shortages closing in on Tajikistan and central Asia', Oxfam, 17 February 2010). One of the worst droughts recorded over India in 2002 shows that the Indian cannot confidently rely on the sporadic seasonal rainfall to supply water, especially when the country is principally agricultural. Monsoon rainfall may not meet the need for a long dry season without a good irrigation system. Due to economic development, groundwater extraction in India has increased over the last several decades. As such, India may face a water shortage problem in the near future (Rodell et al. 2009; Tiwari et al. 2009). Furthermore, the so-called Ganga–Brahmaputra–Meghna (GBM) basins, the world major rainforests amply supplying fresh water to central and south Asia, are also influenced by anomalous climate variations. Chowdhury and Ward (2004) and Jian et al. (2009) show that the sea surface temperature (SST) and El Nino—Southern Oscillation (ENSO) are ones of the factors causing the climate variations here.

Without sufficient ground data to determine water storage variation, space-borne observations may be used for this purpose. The Gravity Recovery and Climate Experiment mission (GRACE; Tapley et al. 2004), launched on March 17, 2002, has provided monthly gravity solutions (GRACE Level 2B) that can be used to infer water storage changes. Recent publications of equivalent water height (EWH) derived from GRACE over central and south Asia suggest that water storage losses occur in this region (Heki and Matsuo 2010; Hwang et al. 2011). These GRACE results are very preliminary and need further verification, especially using in situ and remote sensing measurements. In this paper, we will first enhance the GRACE gravity fields to improve the determination of EWH in central and south Asia (defined in the region: latitude: 15–50°N and longitude: 65–100°E). The data enhancement in this paper will be focused on filtering (de-striping and smoothing) and correcting for the signal leakage and post glacial rebound (PGR) effect to obtain optimal fields of gravity change. Our GRACE result will be compared with the result from a global hydrological model. The EWHs derived from GRACE and the hydrological model at selected climate stations will be assessed using ground-based temperature and precipitation data, and snow water equivalents (SWEs) derived from remote sensing data. The climate stations selected in this study will be from the National Climatic Data Center (NCDC), which provides location (latitude, longitude and altitude) and several types of ground-based climate data. Since many climate stations are terminated after 2002 (GRACE era) in our study region, the stations used in this study are only stations that still provided the climate data between 2002 and 2009. An analysis on the water storage change in central and south Asia based on the correlations between the GRACE-derived EWH and climate data at the climate station locations (grid) will be presented to point out some potential mechanisms of water depletion in this region.

## 2 Gravity change and EWH from GRACE

For the water storage change in this paper, we chose to use the monthly gravity fields of GRACE from Center for Space Research (CSR), University of Texas at Austin, over the

period of April 2002–July 2009. Because of the concern of large uncertainties in the higher degree terms, we used geopotential coefficients up to a maximum degree of 60. CSR did not supply gravity fields in the months of June 2002, July 2002, and June 2003, so the needed monthly gravity values were interpolated linearly from the nearest fields. The $\bar{C}_{10}$ and $\bar{C}_{11}$ values in the CSR gravity fields were replaced by the corrections given by Swenson et al. (2008), and the $\bar{C}_{20}$ values were replaced by the values from satellite laser ranging (SLR) results.

The geopotential coefficients from GRACE beyond a certain degree will need to be calibrated and filtered because of the systematic and random errors contained in the higher degree terms caused by satellite geometry (polar orbit of GRACE) and the aliasing effects due to model errors in ocean tide and atmosphere mass (Wahr et al. 2004). These imperfections produce stripes in the monthly gravity fields, especially along the north–south going ground tracks. Unlike Rodell et al. (2009) who only apply the kernel to their study region without filtering any part of the signal, we decided to use the de-striping (de-correlating) technique of Chambers (2006) and Swenson and Wahr (2006) to reduce the correlations between higher odd and even harmonic degrees and hence the stripes in the GRACE gravity fields. Although a de-striping technique may remove the correlated errors at higher frequency components, there could still be errors left in the de-correlated fields. Therefore, we apply an average Gaussian smoothing (Jekeli 1981; Wahr et al. 1998) to reduce this remaining error. For the de-striping, the odd and even degree for each certain harmonic order or higher was least-squares fitted by a odd or even function, denoted as $f_0(n)$ and $f_e(n)$, respectively. The fitting functions were then removed from the original GRACE coefficients as

$$\bar{C}_{\mathrm{nm}}^{\mathrm{dstrp}}\big|_{s=e,o} = |\bar{C}_{\mathrm{nm}} - f_s(n)|_{n=n_s}^{n_s\,\max}, \quad n \geq m \tag{1}$$

where $\bar{C}_{\mathrm{nm}}^{\mathrm{dstrp}}$ is the de-striped coefficient, $\bar{C}_{\mathrm{nm}}$ is the original coefficient, $f_s(n)$ is the fitting function, which can be even (when $s = e$) or odd (when $s = 0$). The coefficients with degrees from $n_s$ to $n_s$ max are corrected by removing the effects due to the fitting function.

We used polynomials of even and odd degree for the even and odd fitting functions. We experimented with several combinations of polynomial degree and harmonic order to obtain the best result. The best combination is the one that yields the smallest error (in the RMS sense) in EWH over the study region. First, the scale factor for the error of a de-striped coefficient (in this case the $\bar{C}_{\mathrm{nm}}$ coefficient) was computed as (Liu 2008)

$$k_{\mathrm{m}} = \sqrt{\sum_{n=n_0}^{n\,\max}\left(\bar{C}_{\mathrm{nm}}^{\mathrm{dstrp}}\right)^2 \Big/ \sum_{n=n_0}^{n\,\max}\left(\bar{C}_{\mathrm{nm}}\right)^2} \tag{2}$$

where $\bar{C}_{\mathrm{nm}}$ is the original coefficient from the GRACE product, $n_0$ is lowest degree, and $n$ max is the maximum degree for de-striping. The updated error is then

$$\sigma_{\mathrm{nm},\bar{C}}^{\mathrm{dstrp}} = k_{\mathrm{m}}\sigma_{\mathrm{nm},\bar{C}} \tag{3}$$

where $\sigma_{\mathrm{nm},\bar{C}}^{\mathrm{dstrp}}$ is the updated error of GRACE coefficient, $\sigma_{\mathrm{nm},\bar{C}}$ is the error from GRACE product. The updated error of $\bar{S}_{\mathrm{nm}}$ was computed in exactly the same way as for $\bar{C}_{\mathrm{nm}}$ using Eqs. 2 and 3. Since we are concerned with change of gravity field and change of EWH, in reality, the de-striping was applied to the changes of geopotential coefficients (residual geopotential coefficients), $\delta\bar{C}$ and $\delta\bar{S}$, with $\delta\bar{C} = \bar{C}_{\mathrm{nm}} - \bar{C}_{\mathrm{mean}}$ and $\delta\bar{S} = \bar{S}_{\mathrm{nm}} - \bar{S}_{\mathrm{mean}}$,

where $\bar{C}_{\text{mean}}$ and $\bar{S}_{\text{mean}}$ are the average (mean field) of $\bar{C}_{\text{nm}}$ and $\bar{S}_{\text{nm}}$ over April 2002–September 2009.

The error of EWH after de-stripping, $\Delta\sigma^{\text{dstrp}}$, was expanded into a series of spherical harmonics as

$$\Delta\sigma^{\text{dstrp}}(\phi,\lambda) = \frac{a\rho_{\text{ave}}}{3\rho_{\text{w}}}\sum_{n=0}^{\infty}\sum_{m=0}^{n} W_{\text{n}}\frac{2n+1}{1+k_{\text{n}}}\left(\sigma^{\text{dstrp}}_{\text{nm},\bar{C}}\cos m\lambda + \sigma^{\text{dstrp}}_{\text{nm},\bar{S}}\sin m\lambda\right)\bar{P}_{\text{nm}}(\cos\phi) \quad (4)$$

where $\phi$ is co-latitude, $\lambda$ is longitude, $a$ is the mean earth radius, $\rho_{\text{w}}$ is the density of water (1,000 kg/m$^3$), $\rho_{\text{ave}}$ is the average density of the earth (5,517 kg/m$^3$), $k_{\text{n}}$ is the loading Love number of degree $n$, $\sigma^{\text{dstrp}}_{\text{nm},\bar{C}}$ and $\sigma^{\text{dstrp}}_{\text{nm},\bar{S}}$ are the errors of the de-striped coefficients, $\bar{P}_{\text{nm}}$ is the fully normalized Legendre function of degree $n$ and order $m$ and $W_{\text{n}}$ is the 1-D Gaussian smoothing function of degree $n$ (Jekeli 1981; Wahr et al. 1998).

With a 300-km Gaussian smoothing radius, we experimented with polynomial degree 5 and harmonic orders from 8 to 12 for de-striping. With the EWH error of every grid point over the study region computed, the RMS value of the errors over the entire grid was evaluated and given in Fig. 1. In Fig. 1, the RMS values in the increasing order are from P5M10, P5M11, P5M9, P5M8, and P5M12 (see also the comparison over 2006–2007 in the inserted figure of Fig. 1). Figure 1 suggests that the best result of de-striping was obtained in the case of polynomial degree 5 and harmonic degree 10, i.e., the case with P5M10 in Fig. 1 that delivers the smallest RMS errors over April 2002–July 2009. The de-striped residual geopotential coefficients based on P5M10, $\delta\bar{C}^{\text{dstrp}}_{\text{nm}}$ and $\delta\bar{S}^{\text{dstrp}}_{\text{nm}}$, were used to compute the EWH change at each NCDC station location (see Table 1), $\delta\sigma$ by (Hwang and Kao 2006)

$$\delta\sigma(\phi,\lambda) = \frac{a\rho_{\text{ave}}}{3\rho_{\text{w}}}\sum_{n=0}^{\infty}\sum_{m=0}^{n} W_{\text{n}}\frac{2n+1}{1+k_{\text{n}}}\left(\delta\bar{C}^{\text{dstrp}}_{\text{nm}}\cos m\lambda + \delta\bar{S}^{\text{dstrp}}_{\text{nm}}\sin m\lambda\right)\bar{P}_{\text{nm}}(\cos\phi) \quad (5)$$

where all the parameters are defined in the previous equations.

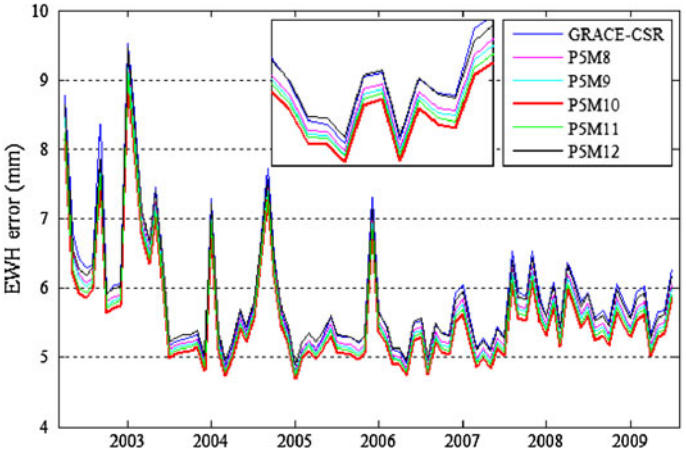


**Fig. 1** Errors of GRACE-derived EWH using different polynomial degrees and orders of spherical harmonic over the study area (latitude: 15–50°N and longitude: 65–100°E), e.g., P5M8 is based on degree 5 polynomial and order 8 of spherical harmonic with a 300-km Gaussian smoothing radius. The *inserted* figure compares the errors over 2006–2007. Ticks of horizontal axis is at January of that year

**Table 1** Stations, coordinates, and scale factors of selected NCDC climate stations

| Station | Latitude (°) | Longitude (°) | Elevation (m) | Scale factor |
|---|---|---|---|---|
| Bayanbulak | 43.033 | 84.150 | 2,459 | 0.898 ± 0.094 |
| Tian Shan | 41.883 | 78.233 | 3,639 | 0.784 ± 0.079 |
| Shiquanhe | 32.500 | 80.083 | 4,280 | 1.711 ± 0.055 |
| Tazhong | 39.000 | 83.667 | 1,099 | 1.185 ± 0.093 |
| Markansu | 39.300 | 73.333 | 4,267 | 0.633 ± 0.060 |
| Hissar | 29.167 | 75.733 | 221 | 0.871 ± 0.090 |
| Pagri | 27.733 | 89.083 | 4,300 | 0.712 ± 0.023 |
| Gauhati | 26.100 | 91.583 | 54 | 1.142 ± 0.035 |
| Bogra | 24.850 | 89.367 | 20 | 1.034 ± 0.027 |

## 3 The hydrological model

Possible independent data sets to validate the surface mass changes measured by GRACE are hydrology models such as the Climate Prediction Center (CPC) model (Fan and Dool 2004), the Land dynamics Model (LaD) model (Milly and Shmakin 2002), and the Global Land Data Assimilation System (GLDAS) model (Rodell et al. 2004). In particular, GLDAS has been widely used in connection with GRACE studies (Andersen and Hinderer 2005; Syed et al. 2008). In this paper, EWH derived from GLDAS was used to assess the GRACE-derived EWH in Sect. 2. Andersen and Hinderer (2005) show that the hydrological model of GLDAS best fits the GRACE equivalent products. The GLDAS products were selected at the same time-window as that of GRACE, with a total of 88 monthly grids between April 2002 and July 2009. In practice, the GLDAS monthly $1^\circ \times 1^\circ$ EWH grids were obtained from the Global Geophysical Fluids Center (GGFC). After subtracting the mean of the monthly fields (average over the 88 months) from each monthly field, residual EWHs were obtained for validation and comparison with GRACE.

Due to de-stripping and smoothing, contamination of the original signals, such as leakage, may occur. In this paper, this problem is reduced using the method of Swenson (2011). In particular, the leakage signal can be restored using a scale factor estimated by the best fit between the original and filtered signals of a well-defined land model such as GLDAS. First, we converted the GLDAS model to the changes of geopotential coefficients as

$$\begin{vmatrix} \delta\bar{C}_{\mathrm{nm}} \\ \delta\bar{S}_{\mathrm{nm}} \end{vmatrix} = \frac{3\rho_{\mathrm{w}}}{4\pi a\rho_{\mathrm{ave}}} \frac{(1+k_{\mathrm{n}})}{(2n+1)} \int \delta\sigma(\varphi,\lambda)\cdot\bar{P}_{\mathrm{nm}}(\cos\phi) \begin{vmatrix} \cos m\lambda \\ \sin m\lambda \end{vmatrix} \sin\phi \mathrm{d}\phi\mathrm{d}\lambda \qquad (6)$$

where $\delta\sigma(\varphi, \lambda)$, $\rho_{\mathrm{w}}$, $\rho_{\mathrm{ave}}$, $a$, $k_{\mathrm{n}}$, $\phi$, and $\lambda$ are already defined in Eq. (4) and Eq. (5). In practice, the integral in Eq. 6 was evaluated discretely by an algorithm described in Hwang and Kao (2006). To ensure that GRACE and GLDAS solutions are compatible, the same maximum harmonic degree of 60 as GRACE was used in Eq. 6. In addition, the coefficients were de-striped and smoothed using the same methods as those used in the GRACE solutions (P5M10 and 300-km radius Gaussian filtering). The filtered GLDAS coefficients were then synthesized at the NCDC station locations (Table 1) using Eq. 5. The scale factor was estimated by minimizing the target function

$$\psi = \left\| \mathbf{b}^{\text{true}} - s\mathbf{b}^{\text{filtered}} \right\|_2 \tag{7}$$

where $\|\cdot\|_2$ is the two-norm, $\mathbf{b}^{\text{true}}$ is a vector of true (original) signal, $\mathbf{b}^{\text{filtered}}$ is a vector of filtered signal, and $s$ is a scale factor. Since GLDAS rather than GRACE is used in the scale factor estimation, we use only one parameter ($s$) to reduce the dependency and bias that may be caused by the model uncertainty of GLDAS. The estimated scale factors are shown in Table 1 (column 5). In our tests, we found that the scale factors are close to one at locations where the EWH variations are small. Here, the filtered GRACE fields are not changed significantly.

After GRACE signal was scaled by the scale factor, PGR correction was applied. PGR correction is retrieved from JPL (http://www.grace.jpl.nasa.gov/data/pgr/), which is based on the model of Paulson et al. (2007); see also Chambers et al. (2010). PGR correction is produced by setting the degree-one terms to zero and applied a 300-km Gaussian filter in the PGR model, which is given as rates of EWH on a 1° × 1° grid.

## 4 The climate data

### 4.1 Precipitation and temperature

In this paper, we used the global, monthly precipitation grids from April 2002 to June 2009 (total 87 grids) supplied by the Global Precipitation Climatology Project (GPCP), available in a binary format at http://www1.ncdc.noaa.gov/pub/data/gpcp/gpcp-v2.1. The web site also provides the reading software. GPCP is under the World Meteorological Organization/World Climate Research Program/Global Energy and Water Experiment (WMO/WCRP/GEWEX). The latest version is GPCP Version 2.1 (Huffman and Bovin 2009; Huffman et al. 2009), which combines data from Special Sensor Microwave/Imager data (SSM/I), merged geosynchronous and low earth orbit infrared data, Outgoing Longwave Radiation (OLR) Precipitation Index (OPI) product, Television Infrared Observation Satellite Operational Vertical Sounder (TOVS) and the Advanced Infrared Sounder (AIRS) information and Global precipitation-gauge products (Huffman et al. 1995; Huffman et al. 2009). The GPCP data have a nominal spatial resolution of 2.5° × 2.5°, and the data are available since January 1979. For comparison with other data on the same locations, the GPCP data were re-sampled on a 1° × 1° grid at a one-month interval. The monthly total precipitation was obtained by multiplying the mean precipitation by the number of days in a month.

The daily temperature data were provided by NCDC at specific stations, complete with latitudes, longitudes, and elevations (Peterson and Vose 1997). The GRACE and GLDAS-derived EWHs and other climate data, which were determined on the regular grids, were interpolated to these stations locations. The daily temperature data were re-sampled at a 1-month interval, and the unit was converted from Fahrenheit to Celsius.

### 4.2 Snow water equivalent

Snow water equivalent (SWE) is the volume of water per unit area that results from the total melting of a snowpack (Brodzik et al. 2007). It is equivalent to the depth of liquid water over the earth surface, much like oceanic tidal height over the oceans. While EWH represents the water storage from the surface to the sub-surface, SWE represents only the water storage from snow. The former also contains the contributions from soil moisture

and underground water. In this paper, we obtained SWE from National Snow and Ice Data Center (NSIDC), which also provides snow-covered areas (SCA) in the world. The SWE from NSDIC is given globally on an equal-area scalable earth (EASE) grid at a 25-km interval. SWE values derived from a passive microwave sensor are subject to the effects of mountainous terrains, vegetations, coastlines, and a number of other factors (Brodzik et al. 2007). In general, anomalously low values of SWE will occur at spots where the microwave measurements are seriously contaminated by the factors listed above. As such, we removed negative values from the raw data and re-sampled the remaining data on a $1^\circ \times 1^\circ$ grid at a 1-month interval. Although SWE from NSDIC is only available up to January 2008, its 6-year time span (2002–2008) is sufficiently long to show the trend of snow-induced water storage change. The relation between SWE and GRACE-derived EWH will be examined later in this paper.

## 5 Results

### 5.1 Trend and correlation analysis

The GRACE- and GLDAS-derived EWHs were compared with climate data at selected NCDC stations (Fig. 2) in central and south Asia to assess water storage changes and detect the possible mechanisms. These stations are permanent NCDC stations and were selected considering the station elevation, climate-sensitivity, and the extent of water storage loss seen in Fig. 2. The data records must also cover the data span of GRACE (from April 2002 to July 2009). Bayanbulak, Tian Shan, Markansu, located near western China, are stations at higher altitudes (2,000–4,000 m). Tazhong is situated at a low-altitude valley surrounded by high mountains. Hissar is a station in northern India, and its elevation is about 221 m. Shiquanhe is close to Hissar, but over a high-mountain region, and it can help to verify various phenomena around this location. Bogra and Gauhati in Bangladesh are located in the GBM Basin, and their elevations are low (<60 m). Like Pagri in the Himalayas, Bogra and Gauhati are also suitable for the investigation of snow melting from the Himalayas because they are in the downstream of Ganges River, which originates from the Himalayas. Located at the high mountains in Tajikistan, Markansu was chosen to see water storage change over central Asia.

Figure 3 shows the times series of EWH derived from GRACE and GLDAS, precipitations, temperatures, and SWE at the NCDC stations. Figure 4 shows the correlation coefficients among these time series. In addition, each the time series was least-squares fitted by the expression:

$$f(\phi, \lambda) = A + B\,t_i + C\cos(\omega t_i) + D\sin(\omega t_i) + E\cos(2\omega t_i) + F\sin(2\omega t_i) \qquad (8)$$

where $A$ represents the offset, $B$ the rate (trend), $C$ and $D$ the annual change, and $E$ and $F$ are the semi-annual change. The rates of the climate records computed from Eq. 8 for all stations are given in Table 2, while the amplitude and phase are given in Table 3. Except at Shiquanhe and Tazhong, the EWHs from GRACE and GLDAS all have negative rates and the two are highly correlated (correlation coefficient $> 0.5$) over the entire time period (see Fig. 4). It is suspected that the poor GLDAS-derived EWHs at Shiquanhe and Tazhong are caused by inadequate observations here when modeling GLDAS. GLDAS-derived EWHs we used in this paper only reflect 4 shallow layers of soil moisture and SWE (Chen et al. 2006); other or deeper layers of hydrological data such as groundwater will possibly be

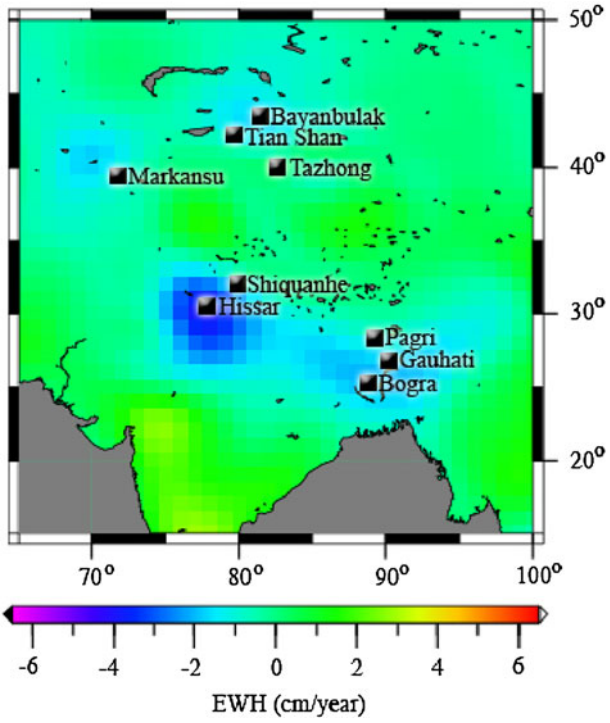


**Fig. 2** Change of EWH (cm/year) over central and south Asia between 2002 and 2009, and selected NCDC climate stations (*dark squares*)

revealed by GRACE only. Therefore, the negative rate of GRACE-derived EWH is most likely caused by groundwater depletion. In verify this, we computed the EWH trend over the same region as Rodell et al. (2009) and obtained a rate of $-3.623 \pm 0.128$ cm/year, which is close to $-4.000 \pm 1.000$ cm/year from Rodell et al. (2009). In addition, the rates of rainfall are negative, and the rates of temperature are positive at most stations. The largest and second largest rainfall rates are found at Gauhati and Bogra. At many stations, especially at low latitudes, the phases of GLDAS-derived EWH, rainfall and temperature are very close to the phases of GRACE-derived EWH.

The increasing rates of the temperatures at the high altitude stations are significantly larger than the average rate given by the Intergovernmental Panel on Climate Change in the last 30 years (IPCC; Pachauri and Reisinger 2007). IPCC shows an average temperature increase of 1–2°C between 1970 and 2004. To confirm our data and analysis results, we also computed the trends of the temperatures at five stations with continuous data (Bayanbulak, Shiquanhe, Hissar, Pagri, and Gauhati) over 1973–2004 (Fig. 5). The trends in Fig. 5 show that the increases of temperatures hardly exceed 1°C over 1973–2004, and this is consistent with the IPCC result. However, the rise of temperature is accelerated after 2000, and this explains why the rates in Table 2 are significantly larger than the IPCC average.

Except at Bayanbulak, the rates of SWE at all high-mountain stations are negative, and there exist correlations between GRACE-derived EWH and SWE. Bayanbulak and Pagri show negative correlations, which could be caused by different physical mechanisms.

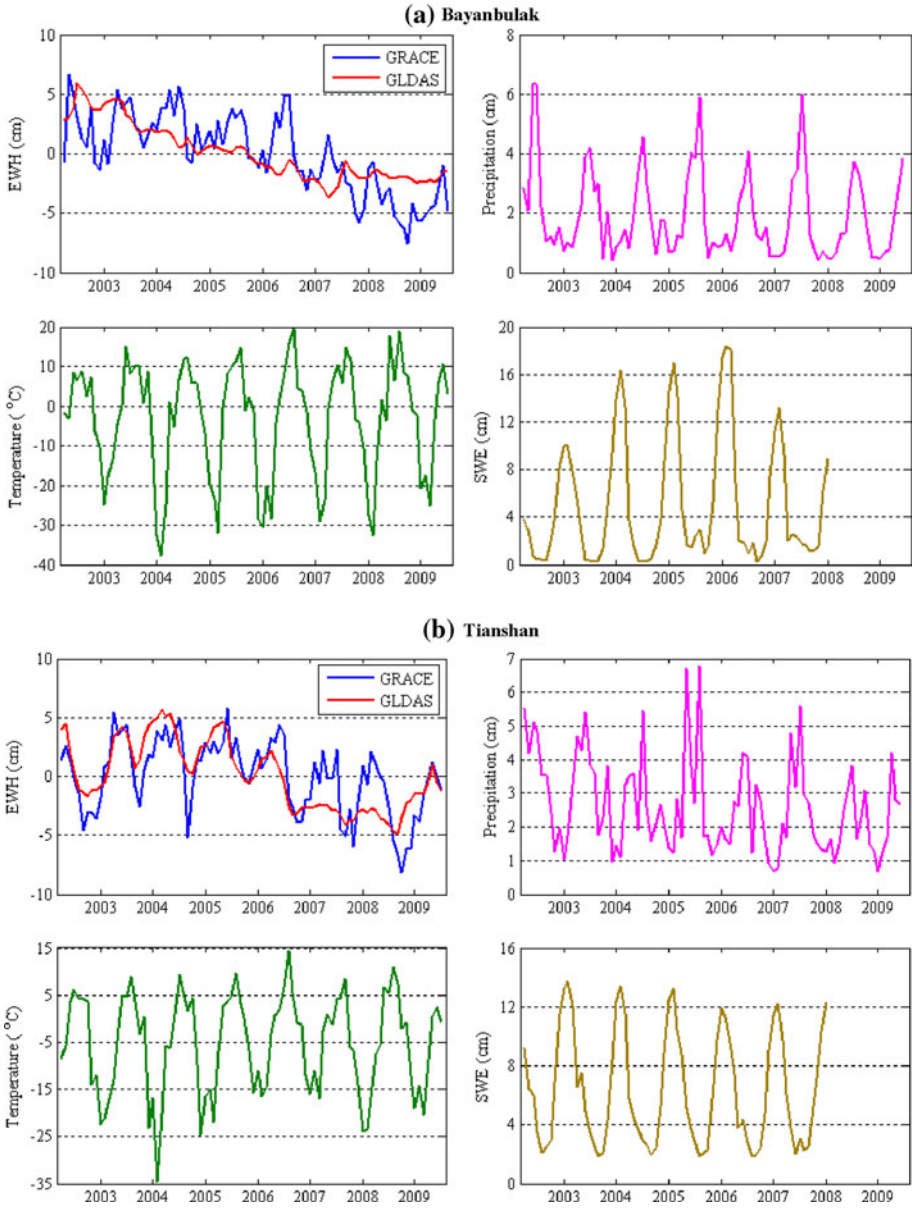


**Fig. 3** Time series of EWH, precipitation, temperature, and SWE. SWE is not available at Tazhong, Hissar, Gauhati, and Bogra. The ticks of the horizontal axis correspond to January

At two neighboring stations with different altitudes, one higher and one lower like at Tian Shan and Bayanbulak, the snow at the lower altitude is likely to be accumulated from the melting of snow at the higher altitude. When the higher altitude snow melts, it moves to the lower altitude and piles up. This causes a negative correlation, and the supporting evidence can be seen from the SWE rate at Bayanbulak, which is positive, while at Tian Shan the

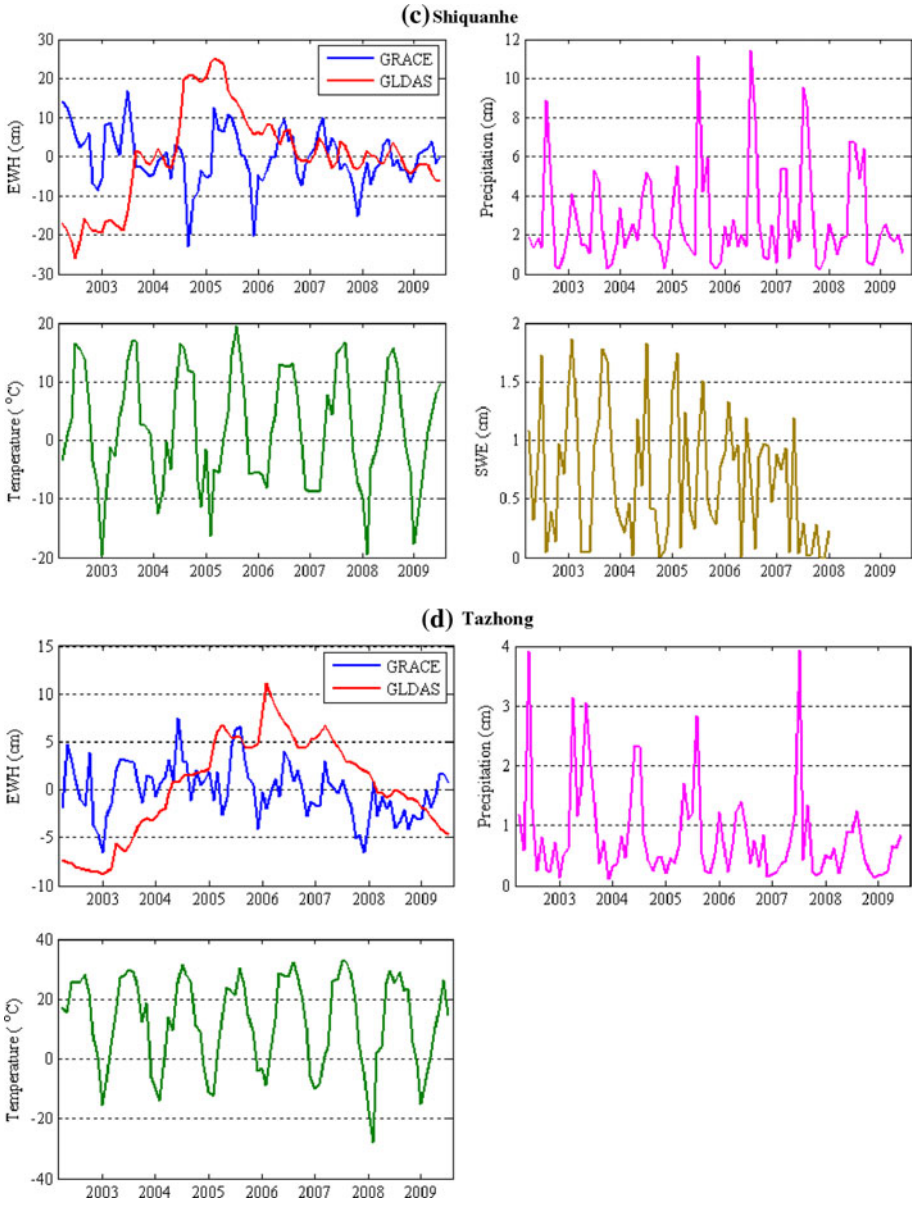


**Fig. 3** continued

rate is negative. GRACE observations around Pagri were contaminated by the leakage from the GBM basins, resulting in a negative correlation between EWH and SWH here (Fig. 4). The negative correlation at Pagri may be explained as follows. In the region around Pagri, the wet season is in fall, and the dry season is in spring. Because GRACE-derived fields have a nominal resolution of about 300 km, the variation of EWH around Pagri will contain a high and a low of the GRACE-derived EWH in fall and spring,

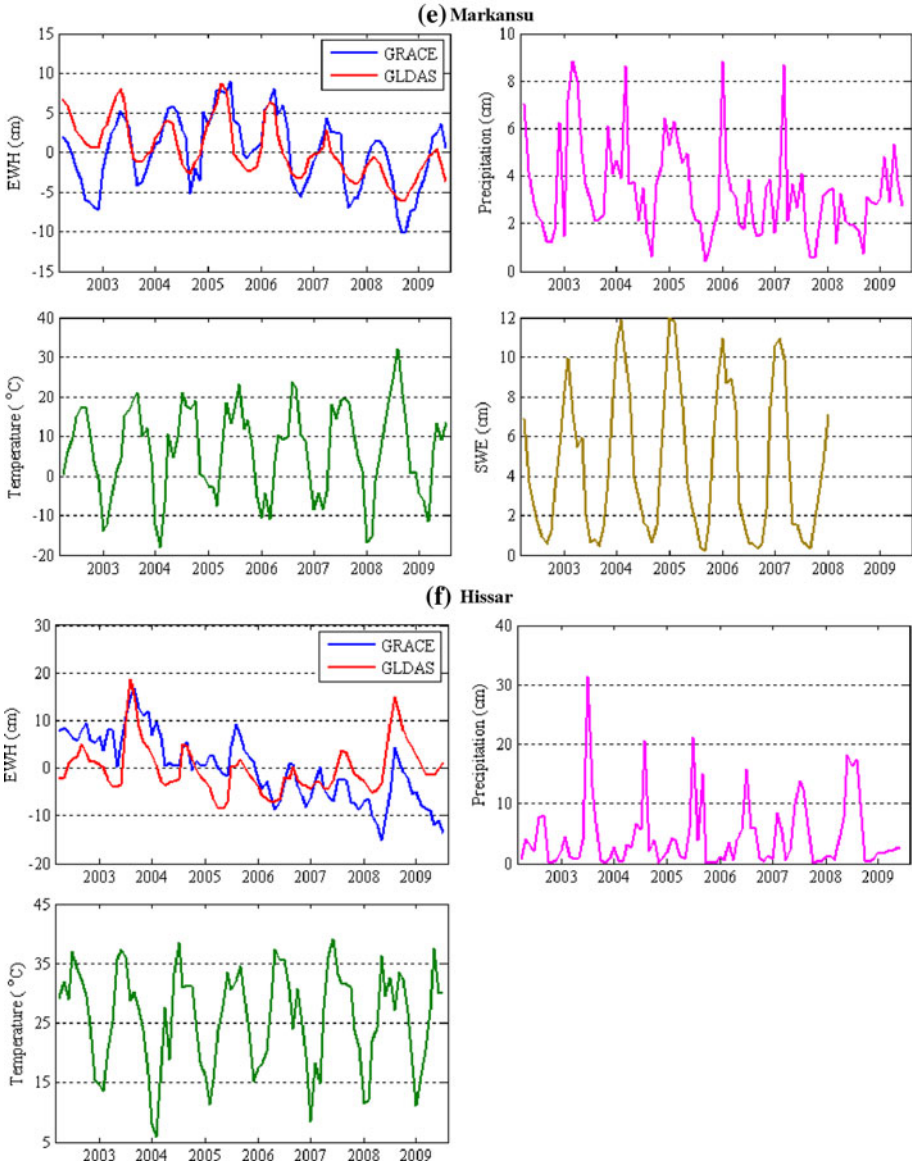


**Fig. 3** continued

respectively. However, the snow at Pagri (note that its elevation is 4,300 m) is accumulated from some time in winter to some time in spring, and then it starts to melt. This results in a high and a low of SWE in spring and fall, respectively. This suggests that SWE is one of the key factors affecting surface mass change over the region. Table 3 also shows that the phase of GRACE-derived EWH is closer to the phase of SWE than to the phase of GLDAS-derived EWH at high latitudes.

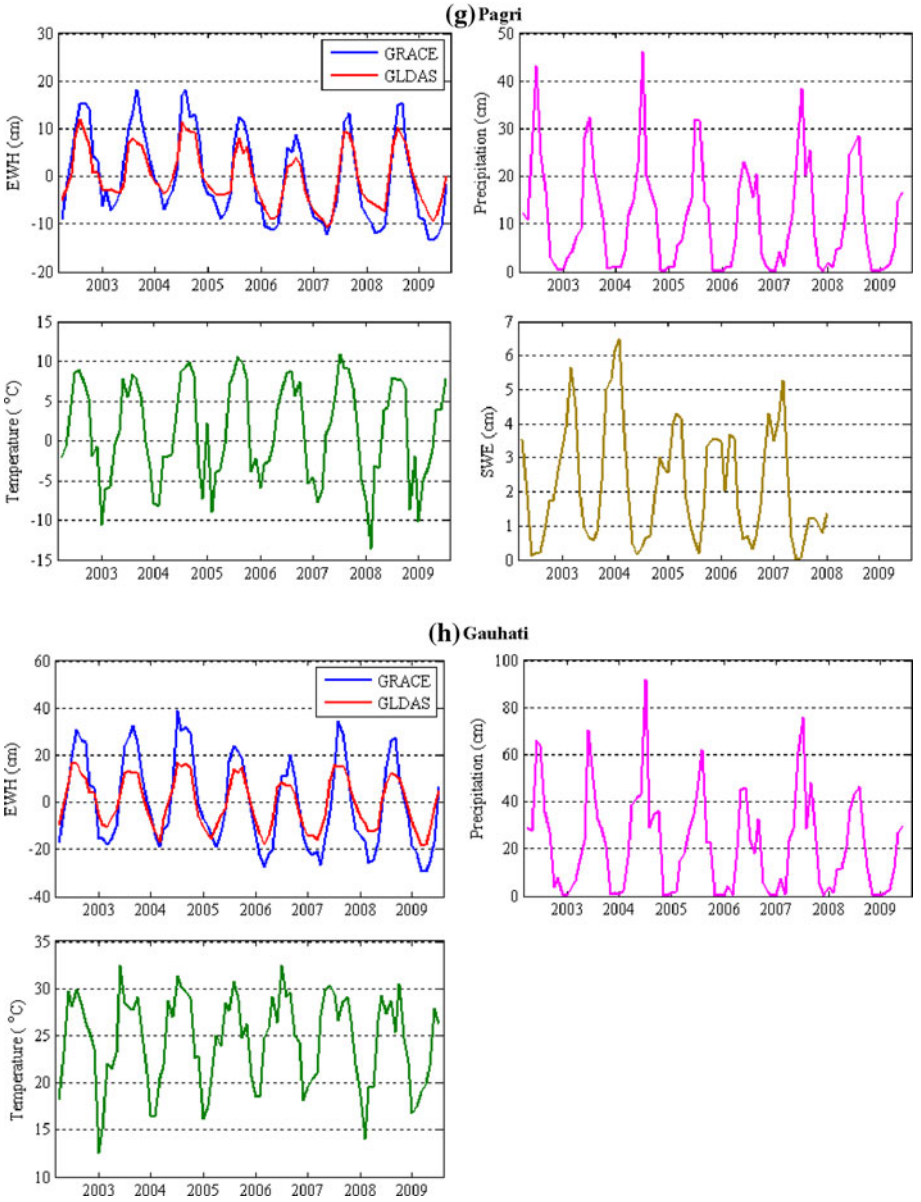


**Fig. 3** continued

Below is a summary of the phenomena seen in Fig. 3:

1. GRACE versus GLDAS: very high correlation is seen at most stations, except at Shiquanhe and Tazhong, where the GLDAS time series undergoes rapid oscillations.
2. GRACE versus precipitation: very high correlation is seen at most stations, except at Hissar. This may be due to the geographical differences that drive different mass transfer rates (e.g., from surface water to groundwater) at each location.

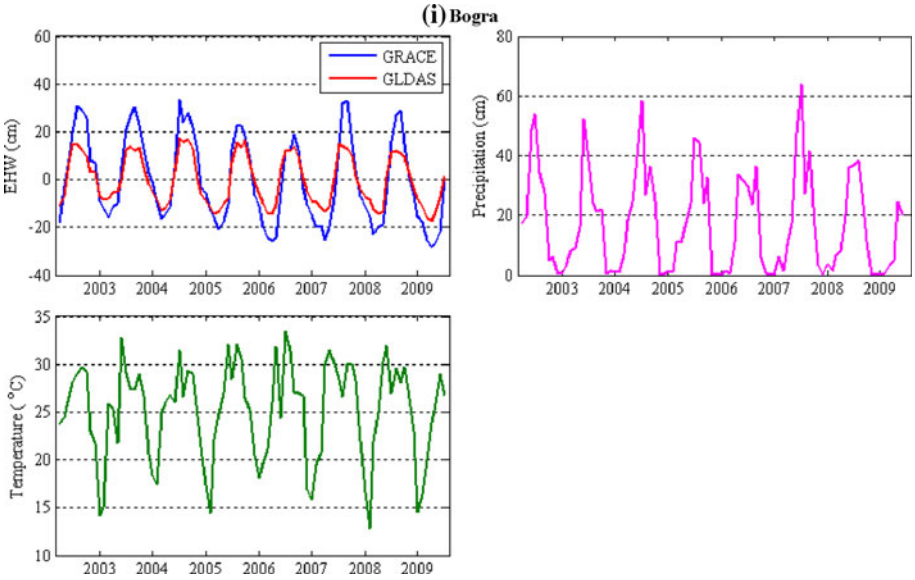


**Fig. 3** continued

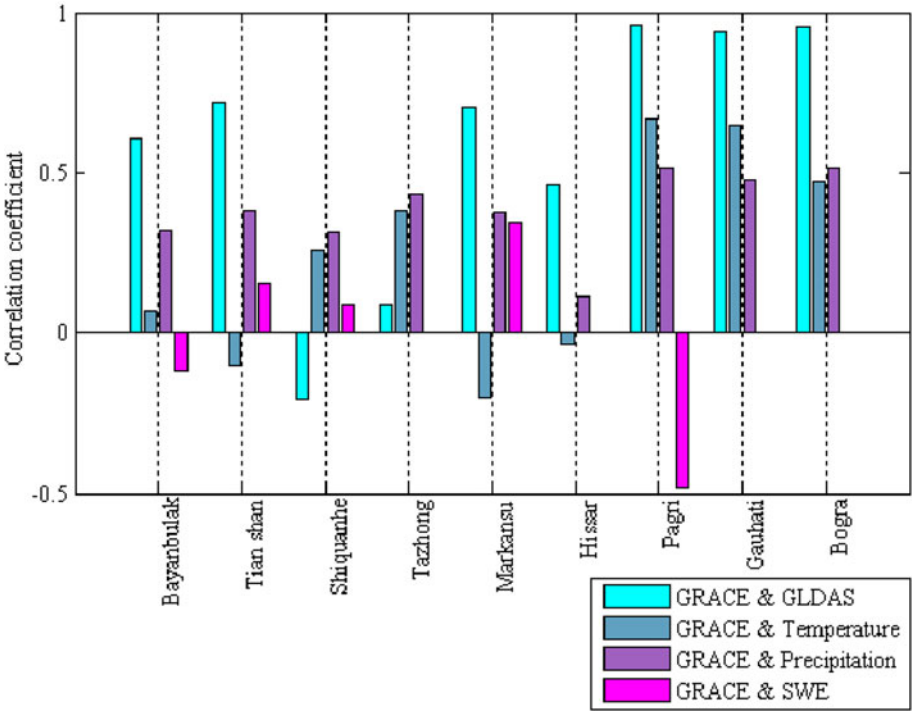


**Fig. 4** Correlation coefficients between GRACE-derived EWH and other climate parameters at the NCDC stations

**Table 2** Rates of EWH, rainfall, temperature, and SWE

| Station | GRACE EWH (cm/year) | GLDAS EWH (cm/year) | Rainfall (cm/year) | Temperature (°C/year) | SWE (cm/year) |
|---|---|---|---|---|---|
| Bayanbulak | −1.182 ± 0.047 | −1.016 ± 0.025 | −0.072 ± 0.019 | 0.273 ± 0.133 | 0.058 ± 0.071 |
| Tian Shan | −0.607 ± 0.051 | −0.900 ± 0.048 | −0.174 ± 0.025 | 0.295 ± 0.095 | −0.203 ± 0.033 |
| Shiquanhe | −0.681 ± 0.132 | 1.560 ± 0.288 | 0.096 ± 0.043 | 0.064 ± 0.080 | −0.080 ± 0.019 |
| Tazhong | −0.388 ± 0.058 | 1.032 ± 0.120 | −0.085 ± 0.016 | −0.200 ± 0.104 | N/A |
| Markansu | −0.452 ± 0.072 | −1.050 ± 0.038 | −0.272 ± 0.038 | 0.383 ± 0.103 | −0.128 ± 0.038 |
| Hissar | −2.644 ± 0.082 | −0.063 ± 0.097 | 0.220 ± 0.101 | 0.151 ± 0.075 | N/A |
| Pagri | −1.298 ± 0.062 | −0.681 ± 0.055 | −0.409 ± 0.108 | 0.046 ± 0.056 | −0.145 ± 0.034 |
| Gauhati | −2.072 ± 0.122 | −0.762 ± 0.083 | −1.001 ± 0.270 | 0.063 ± 0.051 | N/A |
| Bogra | −1.988 ± 0.117 | −0.712 ± 0.071 | −0.500 ± 0.190 | 0.121 ± 0.052 | N/A |

**Table 3** Amplitude and phase of EWH, rainfall, temperature, and SWE

| Station | GRACE EWH (cm, degree) | GLDAS EWH (cm, degree) | Rainfall (cm, degree) | Temperature (°C, degree) | SWE (cm, degree) |
|---|---|---|---|---|---|
| Bayanbulak | 1.678, 292.150 | 0.238, 36.346 | 1.608, 79.744 | 18.274, 86.487 | 6.597, 273.770 |
| Tian Shan | 2.772, 278.395 | 1.604, 281.299 | 1.328, 56.745 | 13.536, 86.615 | 5.175, 272.120 |
| Shiquanhe | 6.034, 298.587 | 1.388, 24.317 | 1.643, 72.771 | 12.967, 87.153 | 0.080, 321.253 |
| Tazhong | 1.997, 36.219 | 0.389, 333.931 | 0.644, 56.879 | 20.085, 87.135 | N/A |
| Markansu | 4.783, 276.538 | 3.297, 274.171 | 1.805, 277.494 | 14.456, 86.793 | 5.062, 272.419 |
| Hissar | 2.614, 78.325 | 4.630, 82.710 | 5.075, 78.202 | 10.206, 85.603 | N/A |
| Pagri | 11.144, 88.065 | 7.173, 87.331 | 14.034, 84.907 | 8.070, 86.830 | 1.959, 276.504 |
| Gauhati | 24.338, 88.242 | 14.088, 87.892 | 25.146, 81.102 | 5.957, 86.103 | N/A |
| Bogra | 23.101, 88.229 | 13.888, 88.197 | 20.843, 84.210 | 6.030, 85.619 | N/A |

3. GRACE versus temperature: very high correlation is seen only at stations over the tropical area, e.g., Pagri, Gauhati, and Bogra. The reason is unknown, but we believe that El Niño may be a cause of this phenomenon (Chowdhury and Ward 2004; Jian et al. 2009).
4. GRACE versus SWE: correlation is seen at most stations where SWE is available, except at Bayanbulak and Pagri. These two exceptions are due to the physical mechanism and signal leakage as mentioned above.
5. At Markansu, the lowest EWH occurred in fall 2008. Also, the rain was the lowest and the temperature was the highest in fall 2008. This is a scientific evidence of the 2008 drought in Tajikistan.

## 5.2 Annual and semi-annual variations

It is important to understand the source that causes the mass loss over central and south Asia region. Since the amplitude and phase of both annual and semi-annual variations derived from GRACE-derived EWH will help to verify the source, the amplitudes and phases of the annual and semi-annual changes on a regular grid were computed and shown in Fig. 6a. Figure 6a suggests that the largest annual and semi-annual changes of EWH

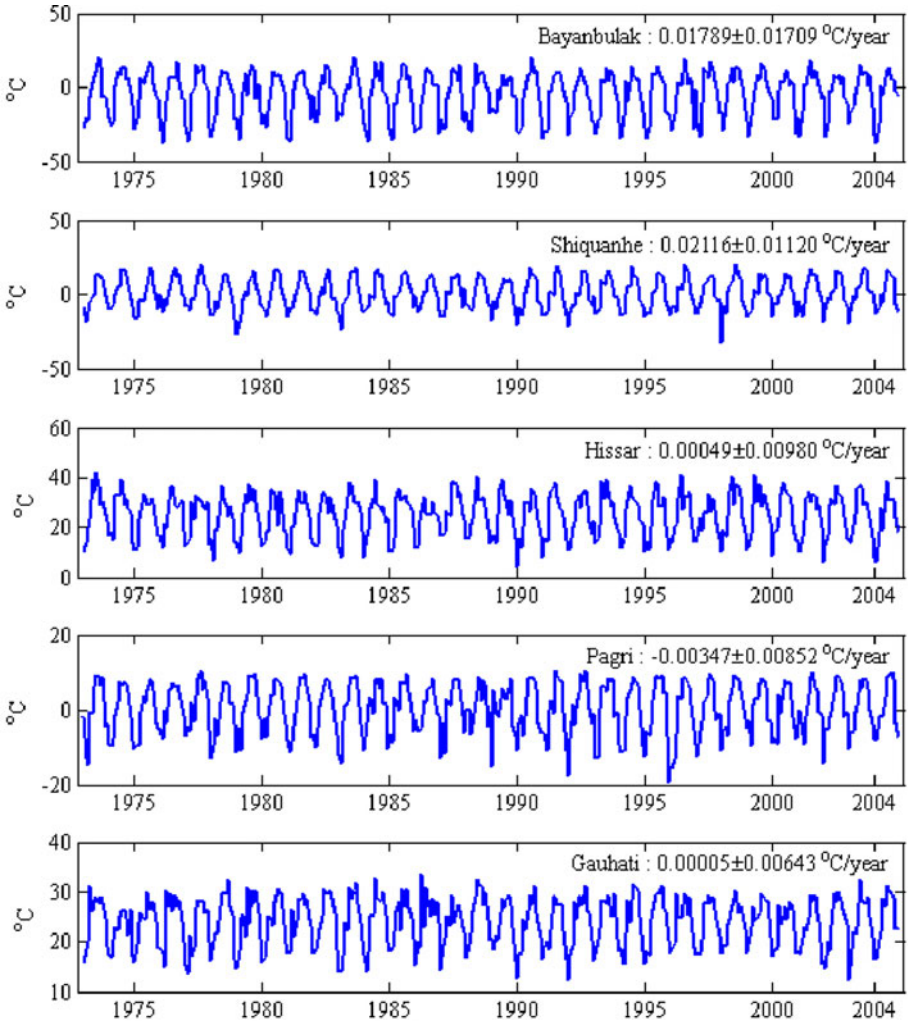


**Fig. 5** Time series of the temperature at five NCDC climate stations over 1973–2004

occur in Bangladesh and northwest India. The phases of such changes are quite uniform throughout the entire India continent. The peak of the annual and semi-annual changes first occurs in the India continent, followed by the mountainous regions to its north. In Fig. 6, a larger phase leads the lesser one in the time of the peak of the annual or semi-annual variation. In general, the low-latitude region leads the high-latitude region in the annual and semi-annual EWH changes. From this relative phase, the snow melting in central Asia may be influenced by the heat from lower latitude, and accelerated warming of the ocean in the last decade may be one of the sources (Shepherd and Wingham 2007). To validate this, the annual and semi-annual variation of the GLDAS hydrology model is also computed and shown in Fig. 6b. The amplitude and phase of GLDAS has a similar pattern as GRACE in the study region.

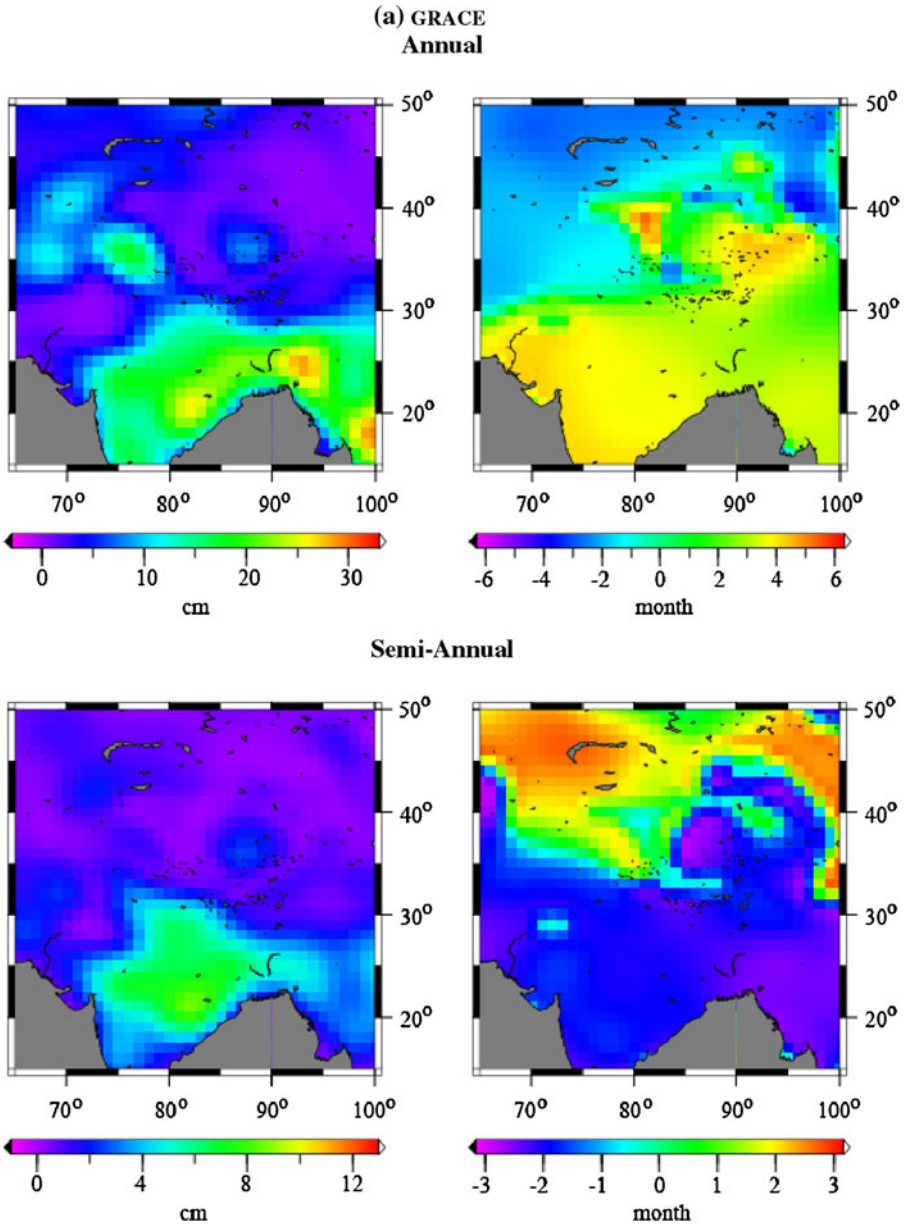


**Fig. 6** **a** Amplitude (*left*) and phase (*right*) of the annual (*top*) and semi-annual (*bottom*) of EWH variation from GRACE. **b** Amplitude (*left*) and phase (*right*) of the annual (*top*) and semi-annual (*bottom*) of EWH variation from GLDAS

### 5.3 Snow melting at high altitude stations

Despite the low reliability in an extremely high-elevation area (Savoie et al. 2009), Fig. 4 shows that SWE data at most stations are correlated with GRACE-derived EWH. To

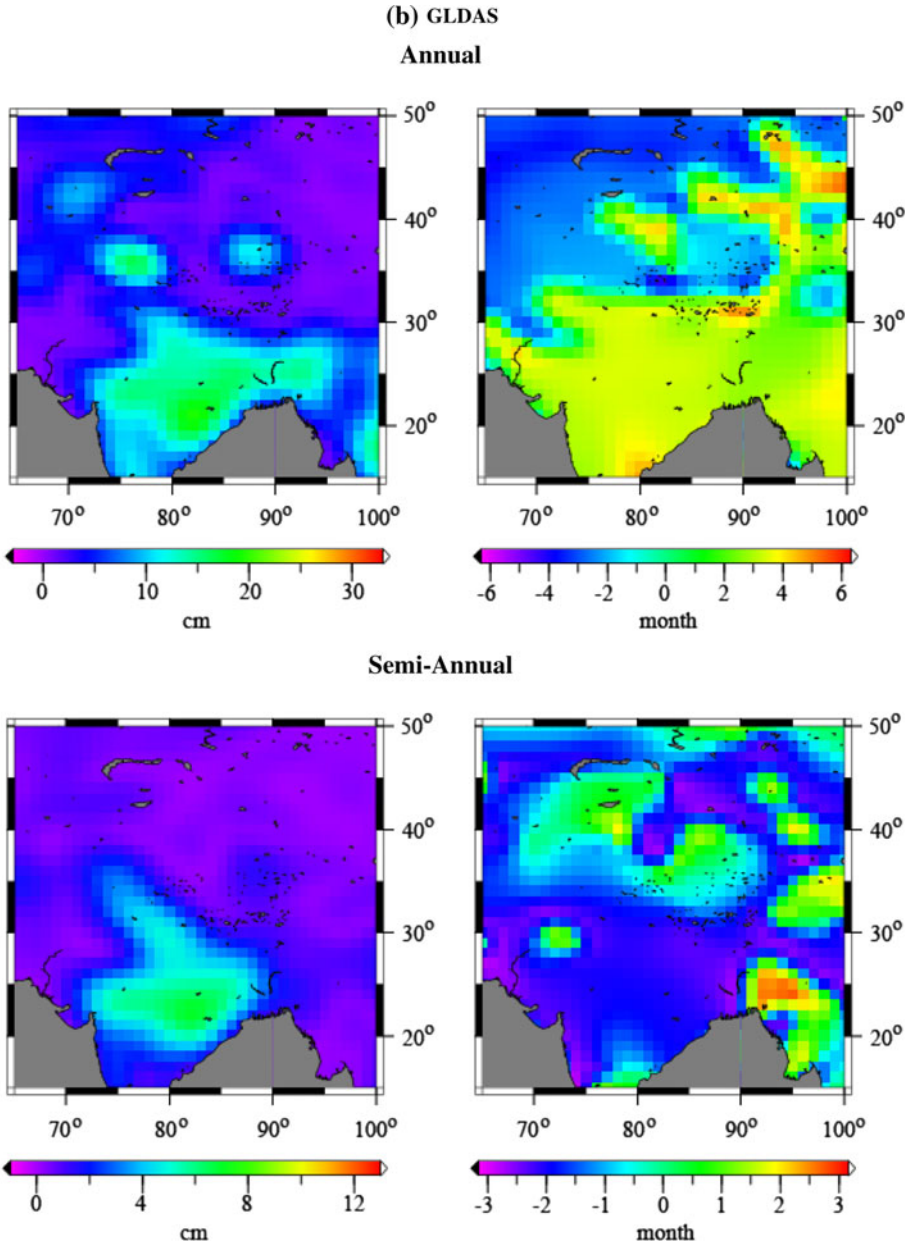


**Fig. 6** continued

validate the GRACE-derived EWH, the rates of SWE from 2002 to 2008 over high-mountain regions were determined. Figure 7 compares the rates of SWE and GRACE-derived EWH. The pattern of the SWE rates (Fig. 7, left) is similar to that of the GRACE-derived EWH rates. However, on average, the EWH rate is roughly an order of magnitude larger. The rates of both are mostly negative, suggesting that both SWE and

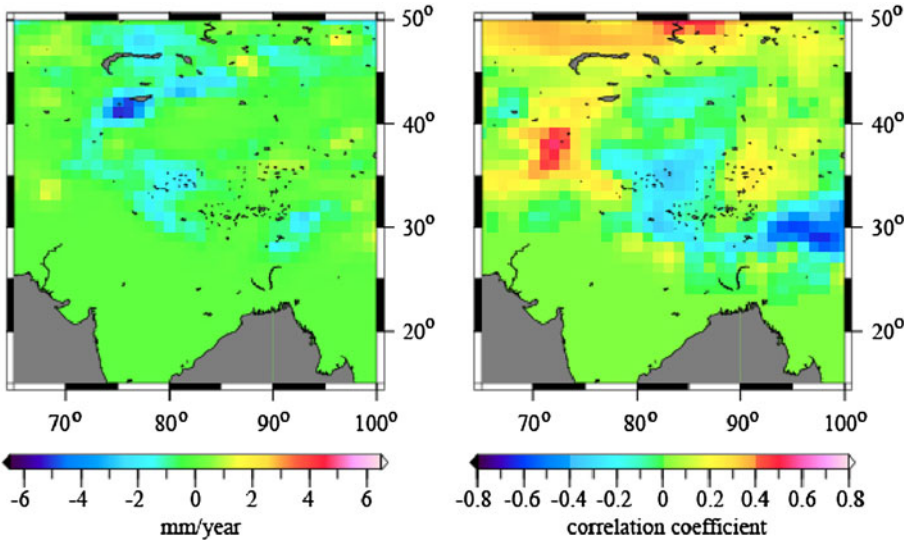


**Fig. 7** Rates (*left*) of SWE over snow-covered regions from April 2002 to January 2008 and correlation coefficient (*right*) between GRACE-derived EWH and SWE

EWH are decreasing here, especially at Markansu where we obtained the largest decreasing rate of snow and the largest increasing rate of temperature. The high spatial correlation between SWE and EWH in Figs. 2 and 7(left) also suggests that melting of snow contributes partly, if not entirely, to the loss of water storage here.

A further demonstration of the correlation between EWH and SWE at high altitudes was made at over the study region. The correlation coefficients between GRACE-derived EWH and SWE are computed at every grid point and plotted in Fig. 7(right). Although the SWE rate is 10 times smaller than the GRACE-derived EWH rate, the correlation coefficients suggest that SWE contributes partly to GRACE-derived EWH. Because SWE is derived from remote sensing data and the resolvable wavelength of GRACE may be coarser than 300 km, the exact contribution of SWE to EWH at the mesoscale wavelength (at about 100 km) is not clear. However, as demonstrated in Figs. 2 and 7, losses of SWE are highly correlated with losses of surface mass at high altitudes. On the other hand, SWE is an efficient hydrological parameter to validate GRACE results over snow-covered regions (Savoie et al. 2009).

### 5.4 Impact of the water loss

The loss of water storage over the study area affects all residents here. For example, in the desert urban like Turpan and Hami, most of the water consumed comes from the groundwater furnished by the melting snow from the high-mountain region over Tian Shan. Acceleration in the increase of temperature accompanied by a significant loss of water storage, as seen in the GRACE and SWE results over 2002–2008, must be closely attended over the Tian Shan and Markansu regions. Although there is no scientific publication released about the cause of mass loss over the region, it is believed that the major cause could be profligate energy consumption of in this region and the neighbors that

produce climate warming to accelerate temperature rise here. The withdrawal of the groundwater in large cities and agriculture areas, especially over the heavily irrigational areas like northern India, may be the major contributor to the water storage loss (Tiwari et al. 2009; Rodell et al. 2009), which is also seen in the GRACE result. If the current trend of EWH loss continues, a major conflict due to water resources is foreseen among the countries in the region and its neighbors.

## 6 Conclusions

We have studied the water storage change over central and south Asia using space-borne observables, hydrology model, and climatology data in this paper. The best combination of filtering with some corrections was employed to extract the best GRACE gravity changes over the region. EWH derived from GRACE and GLDAS is highly correlated at most climate stations of NCDC. Annual and semi-annual variations are mostly occurred at low-latitude areas (<30°), and the phases of such variations depend on geographic locations and elevations. The evidence of global warming can be seen from the temperature rise after 2002, which is several times larger than that in the last century. Due to temperature rises, both EWH and SWE show decreasing trends (especially at Markansu), which lead to continual decreases of surface water storage in the central and south Asia. Over India, the decrease of EWH is also partly caused by significant groundwater usage. The correlation between SWE and EWH over the study region (Fig. 7) suggests that snow melting contributes partly to surface mass change at high-mountain regions.

Although GRACE is a very efficient tool for observing surface mass change over the study region, the global solution (Bettadpur 2007) has a limitation on both temporal and spatial resolutions. Since the study area is over an active tectonic zone, GRACE gravity contains a mixture of geodynamic and hydrological signals, as well as possible aliasing signals due to data processing. This problem is particularly pronounced at the Pagri, Gauhati, and Bogra stations. According to Chen et al. (2009), we can improve the filter used in this paper by performing tests over the tropical oceans where small mass variation is advantageous for selecting an optimal filter. A locally adapted filter may also be used to reduce the loss of possible gravity signatures and leakage problems in the GRACE global solutions. Although the scale factor improves the filtered GRACE fields, it greatly depends on the calibrating model. An improved estimate of scale factor should be based on multiple models. Also, if available, GRACE-derived EWH can be improved by correcting for the tectonic motion effect. Finally, the GRACE uncertainty problem can be mitigated by using a regional GRACE solution such as that give by Wu et al. (2006). These are subjects of future studies.

**Acknowledgments** This study is supported by the National Science Council, and the National Space Organization (NSPO), Taiwan, under the 2010 project "Precise orbit determination and analysis of earth's gravity field from FORMOSAT-3/COSMIC GPS data."

## References

Andersen OB, Hinderer J (2005) Global inter-annual gravity changes from GRACE: early results. Geophys Res Lett 32:L01402. doi:10.1029/2004GL020948

Bettadpur S (2007) Gravity recovery and climate experiment: UTCSR level-2 processing standards document for level-2 product release 0004. Center for Space Research, the University of Texas at Austin

Brodzik MJ, Armstrong R, Savoie M (2007) Global EASE-grid 8-day blended SSM/I and MODIS snow cover (April 2002–January 2008). National Snow and Ice Data Center, Digital media, Boulder

Chambers DP (2006) Evaluation of new GRACE time-variable gravity data over the ocean. J Geophys Res Lett 33:L17603. doi:1029/2006GL027296

Chambers DP, Wahr J, Tamisiea ME, Nerem RS (2010) Ocean mass from GRACE and glacial isostatic adjustment. J Geophys Res 115:B11415. doi:10.1029/2010JB007530

Chen JL, Wilson CR, Famiglietti JS, Rodell M (2006) Attenuation effect on seasonal basin-scale water storage changes from GRACE time-variable gravity. J Geod 23:5–7. doi:10.1007/s00190-006-0104-2

Chen JL, Wilson CR, Tapley BD, Yang ZL, Niu GY (2009) 2005 drought event in the Amazon River basin as measured by GRACE and estimated by climate models. J Geophys Res 114:B05404. doi:10.1029/2008JB006056

Chowdhury MDR, Ward N (2004) Hydro-meteorological variability in the greater Ganges–Brahmaputra–Meghna basins. Int J Climatol 24:1495–1508

Fan Y, Dool VDH (2004) Climate prediction center global monthly soil moisture data set at 0.5° resolution for 1948 to present. J Geophys Res 109:D10102. doi:10.1029/2003JD004345

Heki K, Matsuo K (2010) Time-variable ice loss in Asian high mountains from satellite gravimetry. Earth Planet Sci Lett 290:30–36

Huffman GJ, Bovin DT (2009) GPCP version 2.1 combined precipitation data set document. Laboratory for Atmospheres, NASA Goddard Space Flight Center and Science Systems and Applications, Inc

Huffman GJ, Adler RF, Rudolf B, Schneider U, Keehn PR (1995) Global precipitation estimates based on a technique for combining satellite-based estimates, rain gauge analysis, and NWP model precipitation information. J Climate 8:1284–1295

Huffman GJ, Adler RF, Bolvin DT, Gu G (2009) Improving the global precipitation record: GPCP Version 2.1. Geophys Res Lett 36:L17808. doi:10.1029/2009GL040000

Hwang C, Kao YC (2006) Spherical harmonic analysis and synthesis using FFT: application to temporal gravity variation. Comput Geosci 32:442–451. doi:10.1016/j.cageo.2005.07.006

Hwang C, Kao YC, Tangdamrongsub N (2011) A preliminary analysis of lake level and water storage changes over Lakes Baikal and Balkhash from satellite altimetry and gravimetry. Terr Atmos Ocean Sci 22(2). doi: 10.3319/TAO.2010.05.19.01(TibXS)

Jekeli C (1981) Alternative methods to smooth the earth's gravity field. Report 327. Department of Geodetic Sciences, The Ohio State University, Columbus

Jian J, Webster PJ, Hoyos CD (2009) Large-scale controls on Ganges and Brahmaputra River discharge on intraseasonal and seasonal time-scales. Q J R Meteorol Soc 135:353–370

Liu X (2008) Global gravity field recovery from satellite-to-satellite tracking data with the acceleration approach. Publications on Geodesy 68, Delft

Milly PCD, Shmakin AB (2002) Global modeling of land water and energy balances. Part I: the land dynamics (LaD) model. J Hydrometeorol 3(3):283–299

Niederer P, Bilenko V, Ershova N, Hurni H, Yerokhin S, Maselli D (2008) Tracing glacier wastage in the northern Tien Shan (Kyrgyzstan/central Asia) over the last 40 years. Clim Change 86:227–234. doi:10.1007/s10584-007-9288-6

Pachauri RK, Reisinger A (2007) IPCC fourth assessment report. IPCC, Geneva

Paulson A, Zhong S, Wahr J (2007) Inference of mantle viscosity from GRACE and relative sea level data. Geophys J Int 171:497–508. doi:10.1111/j.1365-246X.2007.03556.x

Peterson TC, Vose RS (1997) An overview of the global historical climatology network temperature database. Bull Am Meteorol Soc 78:2837–2849

Rodell M, Houser PR, Jambor U, Gottschalck J, Mitchell K, Meng CJ, Arsenault K, Cosgrove B, Radakovich J, Bosilovich M, Entin JK, Walker JP, Lohmann D, Toll D (2004) The global land data assimilation system. Bull Am Meteorol Soc 85(3):381–394

Rodell M, Velicogna I, Famiglietti JS (2009) Satellite-based estimates of groundwater depletion in India. Nature 460:999–1002

Savoie MH, Armstrong RL, Brodzik MJ, Wang JR (2009) Atmosphere corrections for improved satellite passive microwave snow cover retrievals over Tibet Plateau. Remote Sens Environ 113:2661–2669

Shepherd A, Wingham D (2007) Recent sea-level contributions of the Antarctic and Greenland ice sheets. Science 315:1529. doi:10.1126/science.1136776

Swenson S (2011) Restoring signal loss in GRACE terrestrial water storage estimates (Draft). Available online at: ftp://podaac.jpl.nasa.gov/pub/tellus/grace_monthly/swenson_destripe/ss201008/doc/

Swenson S, Wahr J (2006) Post-processing removal of correlated errors in GRACE data. J Geophys Res Lett 33:L08402. doi:10.1029/2005GL025285

Swenson S, Chambers DP, Wahr J (2008) Estimating geocenter variations from a combination of GRACE and ocean model output. J Geophys Res Solid Earth 113:B08410. doi:10.1029/2007JB005338

Syed TH, Famiglietti JS, Rodell M, Chen JL, Wilson CR (2008) Analysis of terrestrial water storage changes from GRACE and GLDAS. Water Resour Res 44:W02433. doi:10.1029/2006WR005779

Tapley BD, Bettadpur S, Watkins M, Reigber C (2004) The gravity recovery and climate experiment: mission overview and early results. Geophys Res Lett 31:L09607. doi:10.1029/2004GL019920

Tiwari VM, Wahr J, Swenson S (2009) Dwindling groundwater resources in northern India, from satellite gravity observations. Geophys Res Lett 36:L18401. doi:10.1029/2009GL039401

Wahr J, Molenaar M, Bryan F (1998) Time variability of the Earth's gravity field: hydrological and oceanic effects and their possible detection using GRACE. J Geophys Res Lett 103(B12):30, 205–230, 229

Wahr J, Swenson S, Zlotnicki V, Velicogna I (2004) Time-variable gravity from GRACE: First results. J Geophys Res Lett 31:L11501. doi:10.1029/2004GL019779

Wu SC, Kruizinga G, Bertiger W (2006) Algorithm theoretical basis document for GRACE level-1B data processing V1.2. Jet Propulsion Laboratory, California Institute of Technology